energies

MDPI

Article

Hybrid Extended State Observer with Adaptive Switching Strategy for Overshoot-Free Speed Control and Enhanced Disturbance Rejection in PMSM Drives

Wenwen Lin, Yijie Qian, Wentao Zhang * and Jiaqi Wang

School of Electrical Engineering and Automation, Harbin Institute of Technology, Harbin 150001, China; 23s136593@stu.hit.edu.cn (W.L.); 2022111215@stu.hit.edu.cn (Y.Q.); 2022110580@stu.hit.edu.cn (J.W.)
* Correspondence: zhang_wentaohit@163.com

Abstract

Under complex operating conditions, the single-loop control structure of permanent magnet synchronous motors (PMSMs) suffers from various uncertain disturbances. Although extended state observers with high-gain designs have been widely adopted for disturbance rejection control due to their rapid convergence characteristics, they typically induce significant noise amplification and increased sensitivity to disturbances. To address this issue, this paper proposes a hybrid extended state observer-based control with adaptive switching strategy (AS-HyESO) for suppressing uncertain disturbances. In the AS-HyESO framework, matched disturbances from the control channel and unmatched disturbances from non-control channels are separately estimated using the HyESO, which are subsequently eliminated through the designed control law to ensure precise tracking of the speed reference input. Furthermore, the proposed observer incorporates an adaptive bandwidth switching mechanism that employs larger bandwidth during steady-state operation and reduced bandwidth during dynamic transients. This innovative approach achieves overshoot-free speed regulation while maintaining enhanced disturbance rejection capability, thereby effectively resolving the inherent conflict between dynamic response performance and anti-disturbance robustness. Experimental validation conducted on a 64 W PMSM dual-motor test platform demonstrates the superior effectiveness of the AS-HyESO, control strategy in practical applications.

Keywords: permanent magnet synchronous motor (PMSM); disturbance rejection control; hybrid extended state observer (HyESO); harmonic suppression

check for updates

Academic Editor: Frede Blaabjerg

Received: 29 July 2025
Revised: 18 August 2025
Accepted: 28 August 2025
Published: 31 August 2025

Citation: Lin, W.; Qian, Y.; Zhang, W.; Wang, J. Hybrid Extended State Observer with Adaptive Switching Strategy for Overshoot-Free Speed Control and Enhanced Disturbance Rejection in PMSM Drives. *Energies* **2025**, *18*, 4633. https://doi.org/10.3390/en18174633

Copyright: © 2025 by the authors. Licensee MDPI, Basel, Switzerland. This article is an open access article distributed under the terms and conditions of the Creative Commons Attribution (CC BY) license (https://creativecommons.org/licenses/by/4.0/).

1. Introduction

In recent years, Permanent Magnet Synchronous Motors (PMSMs) have been extensively utilized in transportation [1,2] and industrial automation [3,4] owing to their advantageous characteristics of high torque density, elevated power density, and superior energy conversion efficiency.

However, PMSM drive systems exhibit extensive nonlinear characteristics, including flux harmonics, inverter nonlinearity, parameter mismatch, and imbalanced phase impedance [5]. These factors may induce multi-form disturbances that degrade the control accuracy of PMSM control systems. Furthermore, given the diverse and complex operating conditions of PMSM applications, it is challenging to precisely quantify the number or categorize the specific types of disturbances inherent in the control architecture [6]. Con-

sequently, to enhance the control precision of PMSM-driven systems, it is imperative to investigate suppression techniques targeting these uncertain disturbances.

In recent years, numerous observer-based control schemes grounded in the "estimation–compensation" principle have been developed for disturbance suppression in both current [6,7] and speed loops [8] of PMSM drive systems. Among these methodologies, Active Disturbance Rejection Control (ADRC) has emerged as a prominent solution due to its robust disturbance rejection capability and model-independent characteristics [9]. As the core component of ADRC, the Extended State Observer (ESO) enables real-time estimation of lumped disturbances followed by feedforward compensation, effectively decoupling system dynamics from disturbance influences. To further enhance the robustness of control systems, numerous studies have combined the ESO with sliding mode controllers [10,11]. This integration leverages sliding mode control to handle residual disturbances and high-frequency noise, whereas the ESO reduces the switching gain of sliding mode control, thereby mitigating the chattering issue inherent in traditional sliding mode control.

However, existing research on ESOs remains predominantly confined to dual-loop control architectures in PMSM systems, limiting their application to disturbance suppression within either the current loop or speed loop independently [12]. In such cascaded topologies, the inherent temporal decoupling between the outer speed loop (typically operating at lower sampling frequencies) and the inner current loop (executing high-frequency switching actions) introduces quantization errors and phase misalignment. This temporal incongruity not only induces information loss during inter-loop data transmission but also degrades the synchronization fidelity of disturbance estimation–compensation processes, thereby compromising the system's dynamic performance and robustness against transient disturbances [12,13]. Ref. [14] suggested a single-loop control structure, which demonstrates simplified control design and enhanced parameter tuning convenience to solve these issues.

In single-loop control architectures of PMSMs, the motor dynamics deviate from the non-integral cascade form required for conventional ESO implementation. Furthermore, disturbances entering through non-control input channels—such as load torque variations, parameter mismatches, and unbalanced impedance effects—violate the matched disturbance assumption inherent to traditional ESO frameworks [15]. This structural incompatibility arises because unmatched disturbances propagate through distinct transmission pathways from control inputs, invalidating the disturbance-to-control input channel alignment prerequisite for standard ESO designs. Therefore, it is necessary to improve the traditional ESO to make it applicable to the PMSM single-loop control system. In [15], Li et al. extended the ESO framework by proposing a generalized extended state observer (GESO) applicable to non-integral chain systems. However, this approach only suppresses disturbances associated with current control equations in single-loop architectures, failing to address disturbances introduced by the speed equation.

Besides, the observer's bandwidth exhibits an inverse relationship with the motor's control robustness and dynamic performance. A higher bandwidth compromises control robustness while diminishing disturbance rejection capabilities, whereas a lower bandwidth degrades dynamic responsiveness [8]. Therefore, it is imperative to develop a methodology that reconciles this inherent trade-off, thereby enabling a control system to simultaneously achieve satisfactory dynamic response characteristics and enhanced robustness.

Therefore, this paper suggests an adaptive switching extended state observer (AS-HyESO) framework to overcome the aforementioned issues. It combines the observer's bandwidth adaptive switching strategy with disturbance observation to provide robust management throughout full-speed ranges and strong dynamic response. Figure 1 shows the proposed control diagram of the PMSM drive system.

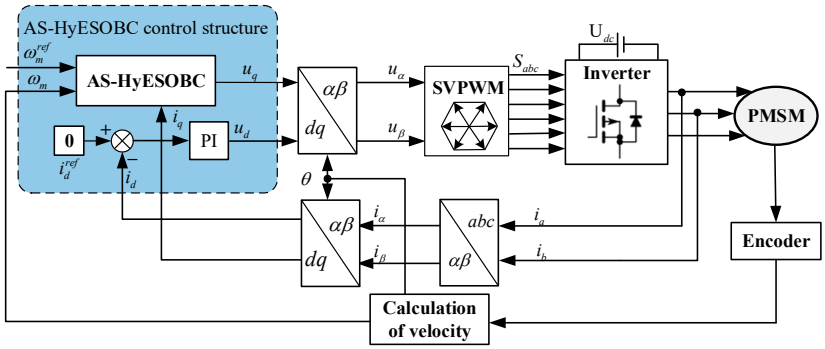


Figure 1. Proposed control diagram of the PMSM drive system.

The key contributions and novelties of this paper are summarized as follows:

(1) The proposed AS-HyESO structure breaks through the limitation of conventional ESOs that can only handle matched disturbances. By employing parallel observation channels to simultaneously estimate matched disturbances in the control input channel and unmatched disturbances in non-control channels, the disturbance rejection scope is extended from the current equation to the entire electromechanical coupling process. This architecture demonstrates significant engineering application value.

(2) The designed transient-identification-based dual-bandwidth switching strategy adopts low bandwidth during transient processes to suppress overshoot while switching to high bandwidth in steady-state operation to enhance disturbance rejection capability. This approach achieves the unification of overshoot-free speed tracking and strong anti-disturbance performance. Furthermore, a concrete parameter configuration scheme for both the controller and observer is provided, significantly simplifying the debugging procedure.

Figure 1 shows the proposed control scheme in this paper. The remaining paper organization is structured as follows: Section 2 provides the mathematical model of PMSM single-loop control with disturbances and the analysis of the design and limitations of traditional ESO. Section 3 focuses on the disturbance compensation algorithm, introducing the HyESO structure. Section 4 details the design of the adaptive control mechanisms. Section 5 validates the control strategy through closed-loop experiments on a hardware platform. Section 6 concludes the paper.

2. Problem Description

2.1. PMSM Single-Loop Control Model Considering Uncertain Aperiodic and Periodic Disturbances

The following form [16] can be used to express the PMSM's mathematical model in the d-q rotating reference frame

$$\begin{cases} \dot{\omega}_m = \frac{K_t i_q}{J} - \frac{B}{J}\omega_m - \frac{T_L}{J} \\ \dot{i}_d = \frac{-R_s i_d + u_d}{L_s} + n_p \omega_m i_q \\ \dot{i}_q = \frac{-R_s i_q + u_q - n_p \psi_f \omega_m}{L_s} - n_p \omega_m i_d \end{cases} \tag{1}$$

where ω_m is the rotational angular velocity. i_d and i_q are the currents on the d- and q-axes. u_d and u_q represent the voltage on the d- and q-axes. R_s, ψ_f, B, L_s, J, n_p are the stator resistance, permanent magnet flux, viscous friction coefficient, synchronous inductance, total inertia, and pole pairs, respectively. The load torque is T_L, and $K_t = 3n_p\psi_f/2$ is the torque constant.

A feasible configuration for the single-loop control system involves utilizing a PI regulator within the d-axis current regulation path, with implementation of zero d-axis current reference assignment to optimize torque-per-ampere efficiency. The structure described in (1) could be simplified through integration of speed regulation functionality into the q-axis current tracking loop, thereby forming a unified control framework.

$$\begin{cases} \dot{\omega}_m = \frac{K_t}{J} i_q - \frac{B}{J}\omega_m - \frac{T_L}{J} \\ \dot{i}_q = -\frac{R_s}{L_s} i_q - \frac{n_p \psi_f}{L_s}\omega_m + \frac{1}{L_s} u_q \end{cases} \tag{2}$$

However, the model described in (2) represents an idealized PMSM configuration, neglecting several nonlinear disturbances that affect practical systems. Key sources of perturbation include parameter mismatches (such as stator resistance variations and inductance deviations), inverter nonlinearities (e.g., dead-time effects and semiconductor voltage drops), phase impedance imbalance, flux linkage harmonics, and unmodeled external disturbances [5]. These disturbances collectively alter the electromagnetic characteristics and dynamic responses of PMSM drives. When systematically accounting for these factors, the PMSM mathematical model can be comprehensively reformulated as follows:

$$\begin{cases} \dot{\omega}_m = \frac{K_t}{J} i_q - \frac{B}{J}\omega_m + d_{\omega-total} \\ \dot{i}_q = -\frac{R_s}{L_s} i_q - \frac{n_p \psi_f}{L_s}\omega_m + \frac{1}{L_s} u_q + d_{q-total} \end{cases} \tag{3}$$

where $d_{\omega-total}$ and $d_{q-total}$ stand for the mechanical equation and the q-axis total disturbance, respectively. The variables and their derivatives have finite bounds, and these quantities are differentiable [15].

Based on the dynamic characteristics of disturbance effects, the disturbances in (3) can be classified into two fundamental categories [17]: aperiodic disturbances and periodic disturbances. This classification enables systematic disturbance modeling for PMSM control systems

$$\begin{cases} d_{\omega-total} = d_{\omega-ap} + d_{\omega-p} \\ d_{q-total} = d_{q-ap} + d_{q-p} \end{cases} \tag{4}$$

where $d_{(\cdot)-ap}$ denote the aperiodic disturbances, and $d_{(\cdot)-p}$ correspond to the periodic disturbances.

From (2) to (4), the aperiodic disturbances of the mechanical equation and the q-axis can be written as follows:

$$\begin{cases} d_{\omega-ap} = \frac{K_t}{J} i_q - \frac{B}{J}\omega_m - \frac{T_L}{J} + \Delta_{\omega-ap} \\ d_{q-ap} = -\frac{R_s}{L_s} i_q - \frac{n_p \psi_f}{L_s}\omega_m + \frac{1}{L_s} u_q + \Delta_{q-ap} \end{cases} \tag{5}$$

where $\Delta_{\omega-ap}$ and Δ_{q-ap} are the mechanical equation and the q-axis unknown aperiodic disturbances.

2.2. Traditional Extended State Observer and Its Limitations

A 2nd-order single-input single-output (SISO) system can be represented in the form of an integral chain structure as follows:

$$\begin{cases} \dot{x}_1 = x_2 \\ x_2 = f(x_1, x_2) + \alpha u \\ y = x_1 \end{cases} \tag{6}$$

where each state x_i corresponds to the integral of the subsequent state x_{i+1}, ultimately driven by the system's lumped disturbance $f(\cdot)$ and input coupling term αu, where α is

the coefficient of the control input, and u is the control input. The output y is directly observable from the first state variable.

By treating the lumped disturbance term $f(\cdot)$ as an extended state variable, the state equations based on extended states can be expressed as

$$\begin{cases} \dot{x}_1 = x_2 \\ x_2 = f(x_1, x_2) + \alpha u \\ x_3 = f(x_1, x_2) \\ y = x_1 \end{cases} \tag{7}$$

To estimate the lumped disturbance in (2), the conventional ESO can be formulated as

$$\begin{cases} \dot{z}_1 = z_2 - \beta_1(z_1 - y) \\ \dot{z}_2 = z_3 + \alpha u - \beta_2(z_1 - y) \\ \dot{z}_3 = -\beta_3(z_1 - y) \end{cases} \tag{8}$$

where $z_i (i = 1, 2, 3)$ are the estimated states of the system (7) and $\beta_i (i = 1, 2, 3)$ are the feedback control gains of the ESO.

By appropriately selecting the ESO's control feedback gains, the traditional ESO-based control (ESOBC) is designed as

$$u = kx - \frac{z_{n+1}}{\alpha} \tag{9}$$

where k is the gain vector of the nominal state feedback controller.

Set $\omega_m = x_1$ and $i_q = x_2$, and (3) can be transformed to

$$\begin{cases} \dot{x}_1 = \frac{K_t}{J} x_2 - \frac{B}{J} x_1 + d_{\omega-total} \\ \dot{x}_2 = -\frac{R_s}{L_s} x_1 - \frac{n_p \psi_f}{L_s} x_2 + \frac{1}{L_s} u_q + d_{q-total} \\ y = x_1 \end{cases} \tag{10}$$

Comparing (10) with (6), the PMSM single-loop control system considered in (10) does not conform to the traditional integral chain form described in (6). Secondly, disturbances are not only present in the equations of the control input channel u_q but also in other channels of u_q. Disturbances entering the system through the control input channel $d_{q-total}$ are referred to as 'matched' disturbances. Disturbances entering the system through different channels of $d_{\omega-total}$ are referred to as 'unmatched' disturbances. For a single traditional ESO, it is not possible to estimate both matched and unmatched types of multi-channel disturbances [15].

Therefore, it is necessary to design a hybrid extended state observer to solve the problem of suppressing disturbances in different input channels and improve the robustness of the PMSM control system.

3. Hybrid Extended State Observer Design (HyESO)

3.1. HyESO for Mismatched Disturbance

Without creating the control input u_q from (10), it is possible to define the PMSM single-loop subsystem with the mismatched components.

$$\begin{cases} \dot{\omega}_m = \frac{K_t}{J} i_q - \frac{B}{J} \omega_m + d_{\omega-total} \\ y_{mm} = \omega_m \end{cases} \tag{11}$$

where y_{mm} represents the observable output in the speed control channel.

Similar to the traditional ESO, considering $d_{\omega-total}$ as an extended state variable, the augmented state-based dynamic equation is given by

$$\begin{cases} \dot{\omega}_m = \frac{K_t}{J} i_q - \frac{B}{J}\omega_m + d_{\omega-total} \\ \dot{x}_{mm} = \dot{d}_{\omega-total} \end{cases} \tag{12}$$

Based on (12), HyESO for mismatched disturbance can be constructed as

$$\begin{cases} \begin{bmatrix} \dot{\hat{\omega}}_m \\ \dot{\hat{x}}_{mm} \end{bmatrix} = \begin{bmatrix} -\frac{B}{J} & 1 \\ 0 & 0 \end{bmatrix} \begin{bmatrix} \hat{\omega}_m \\ \hat{x}_{mm} \end{bmatrix} + \begin{bmatrix} \frac{K_t}{J} i_q \\ 0 \end{bmatrix} + L_{mm}(y_{mm} - \hat{y}_{mm}) \\ \hat{y}_{mm} = \hat{\omega}_m \end{cases} \tag{13}$$

where $\hat{\omega}_m$ and $\hat{x}_{mm}$ are the estimated quantities of the state variables ω_m and x_{mm}. Matrix L_{mm} is the required mismatched observer gain for the proper estimation.

3.2. HyESO for Matched Disturbance

With the control input u_q from (10), it is possible to define the PMSM single-loop subsystem with the matched components.

$$\begin{cases} \dot{i}_q = -\frac{R_s}{L_s} i_q - \frac{n_p \psi_f}{L_s}\omega_m + \frac{1}{L_s} u_q + d_{q-total} \\ y_m = i_q \end{cases} \tag{14}$$

where y_m represents the observable output in the current control channel.

Similar to the traditional ESO, considering $d_{q-total}$ as an extended state variable, the augmented state-based dynamic equation is given by

$$\begin{cases} \dot{i}_q = -\frac{R_s}{L_s} i_q - \frac{n_p \psi_f}{L_s}\omega_m + \frac{1}{L_s} u_q + d_{q-total} \\ \dot{x}_m = \dot{d}_{q-total} \end{cases} \tag{15}$$

Based on (15), HyESO for matched disturbance can be constructed as

$$\begin{cases} \begin{bmatrix} \dot{\hat{i}}_q \\ \dot{\hat{x}}_m \end{bmatrix} = \begin{bmatrix} -\frac{R_s}{L_s} & 1 \\ 0 & 0 \end{bmatrix} \begin{bmatrix} i_q \\ \hat{x}_{mm} \end{bmatrix} + \begin{bmatrix} -\frac{n_p \psi_f}{L_s}\omega_m \\ 0 \end{bmatrix} + \begin{bmatrix} \frac{1}{L_s} \\ 0 \end{bmatrix} u_q + L_m(y_m - \hat{y}_m) \\ \hat{y}_m = \hat{i}_q \end{cases} \tag{16}$$

where $\hat{i}_q$ and $\hat{x}_m$ are the estimated quantities of the state variables i_q and x_m. Matrix L_m is the required matched observer gain for the proper estimation.

3.3. The Design of HyESO-Based Control

This section develops a composite feedback control law to achieve dual objectives of high-fidelity input trajectory tracking and coordinated suppression of multi-loop coupled disturbances in the drive system. The dynamics of the system (3) can be expressed as a function of the estimated states using HyESO by

$$\begin{cases} \dot{\hat{\omega}}_m = \frac{K_t}{J} \hat{i}_q - \frac{B}{J}\hat{\omega}_m + \hat{d}_{\omega-total} \\ \dot{\hat{i}}_q = -\frac{R_s}{L_s} \hat{i}_q - \frac{n_p \psi_f}{L_s}\hat{\omega}_m + \frac{1}{L_s} u_q + \hat{d}_{q-total} \\ \hat{y}_c = \hat{\omega}_m \end{cases} \tag{17}$$

By integrating the matched and unmatched disturbance components in Sections 3.1 and 3.2, the state estimation error equation for the entire PMSM system can be derived as follows:

$$\dot{e} = \begin{bmatrix} A_{mm} - L_{mm}C_{mm} & 0 \\ 0 & A_m - L_m C_m \end{bmatrix} e + \begin{bmatrix} -E_{mm} & 0 \\ 0 & -E_m \end{bmatrix} \begin{bmatrix} x_{mm} \\ x_m \end{bmatrix} \tag{18}$$

where matrices $A_{mm} = \begin{bmatrix} -\frac{B}{J} & 1 \\ 0 & 0 \end{bmatrix}$, $A_m = \begin{bmatrix} -\frac{R_s}{L_s} & 1 \\ 0 & 0 \end{bmatrix}$, $C_{mm} = C_m = \begin{bmatrix} 1 & 0 \end{bmatrix}$, $E_{mm} = E_m = \begin{bmatrix} 1 \\ 0 \end{bmatrix}$. The variable e represents the composite error of the integrated system, encapsulating both matched components and mismatched components. Set $d = \begin{bmatrix} d_{\omega-total} \\ d_{q-total} \end{bmatrix}$, then,

$$e = \hat{d} - d \tag{19}$$

Based on (18), the extended system dynamics can be expressed by

$$\begin{bmatrix} \dot{\hat{x}} \\ \dot{e} \end{bmatrix} = \begin{bmatrix} A & I_2 \\ 0 & A_e \end{bmatrix} \begin{bmatrix} \hat{x} \\ e \end{bmatrix} + \begin{bmatrix} B \\ 0 \end{bmatrix} + \begin{bmatrix} I_2 & 0 \\ 0 & E \end{bmatrix} \begin{bmatrix} d \\ \dot{d} \end{bmatrix} \tag{20}$$

where $\hat{x} = \begin{bmatrix} \hat{\omega}_m \\ \hat{i}_q \end{bmatrix}$, $A = \begin{bmatrix} -\frac{B}{J} & \frac{K_t}{J} \\ -\frac{n_p \psi_f}{L_s} & -\frac{R_s}{L_s} \end{bmatrix}$, $A_e = \begin{bmatrix} A_{mm} - L_{mm}C_{mm} & 0 \\ 0 & A_m - L_m C_m \end{bmatrix}$, $I_2 = \begin{bmatrix} 1 & 0 \\ 0 & 1 \end{bmatrix}$ $B = \begin{bmatrix} 0 \\ \frac{1}{L_s} \end{bmatrix}$, $E = \begin{bmatrix} -E_{mm} & 0 \\ 0 & -E_m \end{bmatrix}$.

Three gains—reference input gain (Θ_r), disturbance compensation gain (Θ_d), and state feedback gain (Θ_k)—are defined in order to get strong disturbance immunity and target tracking capacity. The control law in this work is created by combining these three gains as

$$u_q = \Theta_r \omega_m + \Theta_k \begin{bmatrix} \hat{\omega}_m \\ \hat{i}_q \end{bmatrix} - \Theta_d \begin{bmatrix} d_{\omega-total} \\ d_{q-total} \end{bmatrix} \tag{21}$$

The reference input gain (Θ_r) and disturbance compensation gain (Θ_d) can be defined as

$$\Theta_r = -\left[G_1 {G_2}^{-1} B \right]^{-1} \tag{22}$$

$$\Theta_d = -\left[G_1 {G_2}^{-1} B \right]^{-1} \times \left[G_1 {G_2}^{-1} I_2 \right] \tag{23}$$

where $G_1 = \begin{bmatrix} 1 & 0 \end{bmatrix}$, $G_2 = A - B\Theta_k$.

Figure 2 shows the detail of the proposed HyESO based controller.

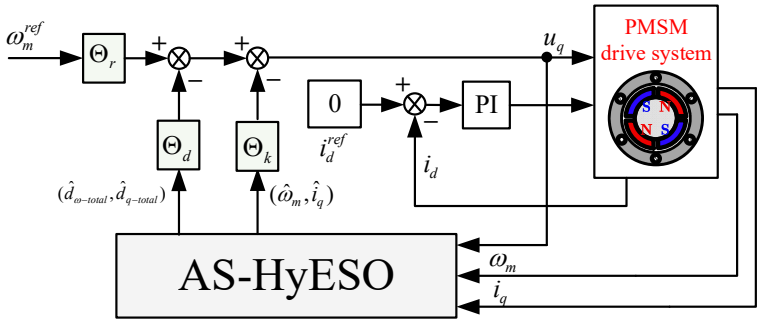


Figure 2. Design of the HyESO-based controller.

Substituting (21) into (20), the extended dynamics are defined as

$$\begin{bmatrix} \dot{\hat{x}} \\ \dot{e} \end{bmatrix} = \begin{bmatrix} \boldsymbol{G}_2 & I_2 - B\Theta_d \\ 0 & A_e \end{bmatrix} \begin{bmatrix} \hat{x} \\ e \end{bmatrix} + \begin{bmatrix} B\Theta_r \\ 0 \end{bmatrix} \omega_m + \begin{bmatrix} I_2 - B\Theta_d & 0 \\ 0 & E \end{bmatrix} \begin{bmatrix} \hat{d} \\ \dot{d} \end{bmatrix} \tag{24}$$

According to (24), the simplified equation for the estimated state can be expressed as

$$\begin{cases} \dot{\hat{x}} = \boldsymbol{G}_2 \hat{x} + B\Theta_r \omega_m + (I_2 - B\Theta_d)\hat{d} \\ \hat{y}_c = C\hat{x} \end{cases} \tag{25}$$

where $C = [1 \quad 0]$.

From (25), the values of the estimated state variables and output state variables can be obtained as

$$\begin{cases} \hat{x} = \boldsymbol{G}_2{}^{-1}\left[\dot{\hat{x}} - B\Theta_r \omega_m - (I_2 - B\Theta_d)\hat{d}\right] \\ \hat{y}_c = C\boldsymbol{G}_2{}^{-1}\left[\dot{\hat{x}} - B\Theta_r \omega_m - (I_2 - B\Theta_d)\hat{d}\right] \end{cases} \tag{26}$$

Appropriate selection of observer gains $L = \begin{bmatrix} L_{mm} \\ L_m \end{bmatrix}$ will respectively ensure the asymptotic convergence of the proposed HyESO against mismatched and matched concentrated disturbances. Since matrix $\boldsymbol{G}_2$ and matrix A_e are Hurwitz, matrix $\begin{bmatrix} \boldsymbol{G}_2 & I_2 - B\Theta_d \\ 0 & A_e \end{bmatrix}$ is also Hurwitz. So, the HyESO-based PMSM control system is asymptotically stable.

Assuming the HyESO designed for multi-channel lumped disturbances has converged to a constant d_s, according to the theorems in [15], in the steady state, the following equation can be obtained:

$$\lim_{t\to\infty} \dot{\hat{x}} = 0, \lim_{t\to\infty} \hat{x} = \lim_{t\to\infty} x, \lim_{t\to\infty} \dot{e} = 0, \lim_{t\to\infty} \hat{d} = d_s \tag{27}$$

Based on (22), (23), (26), and (27), the output can be written as

$$\lim_{t\to\infty} y_c = \omega_m \tag{28}$$

(28) shows that the proposed control scheme can achieve tracking control in the presence of expected reference input ω_m.

4. Adaptive Control for HyESO

The selection of observer gain parameters L_{mm} and L_m significantly impacts the performance of the PMSM system [8]. According to [18], the characteristic equations for both matched and unmatched components in HyESO can be expressed as

$$\det[sI - (A_{mm} - L_{mm}C_{mm})], \det[sI - (A_m - L_m C_m)] \tag{29}$$

where I represents identity matrix.

To reduce the parameter tuning complexity of the system, all roots of the characteristic equation are positioned at $-\omega_0$ based on the method in [19], and the HyESO's observer gain can be expressed as

$$L = \begin{bmatrix} L_{mm} \\ L_m \end{bmatrix} = \begin{bmatrix} 2\omega_0 \\ {\omega_0}^2 \\ 2\omega_0 \\ {\omega_0}^2 \end{bmatrix} \tag{30}$$

where ω_0 is the bandwidth of the HyESO.

According to [20,21], the observer's dynamic performance will suffer if ω_0 is too small, while the system's robustness will be impacted, and system divergence may result if ω_0 is too big. The rise time will be enhanced with the increase of ω_0. However, the negative impact of high gain is also apparent, leading to excessive overshoot and large fluctuations caused by noise amplification, which are unacceptable [22]. To reconcile the inherent trade-off between dynamic responsiveness and disturbance rejection, an adaptive switching observer according to the tracking error and setting time of estimation has been developed.

The flowchart of switching logic is shown in Figure 3. The adaptive switching process can be partitioned into three distinct phases: the transient phase, delay phase, and steady-state phase. The bandwidth of HyESO1 is larger than HyESO2. It employs a smaller observer bandwidth during transient motor dynamics to prioritize rapid error convergence and reduce overshoot while implementing a reduced observer bandwidth in steady-state operations to optimize harmonic suppression and noise immunity.

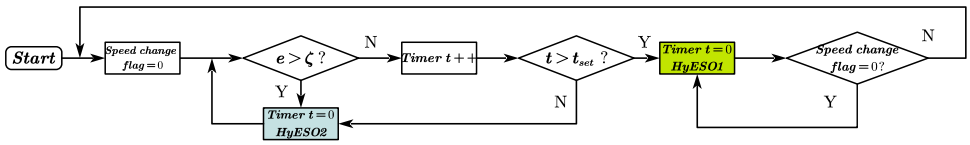


Figure 3. Flowchart of switching logic.

The adaptive work process can be summarized as follows:

(1) The Speed change flag serves as a status indicator for whether the motor needs to execute a speed change process. When Speed change flag = 0, it indicates that no speed adjustment is required for the motor. The parameter is automatically updated to Speed change flag = 1 when a variation in reference speed occurs, signifying that the motor must initiate the speed transition procedure.

(2) Dynamic state: Define the threshold value ζ. If $e > \zeta$, it can be assumed that the motor is in a dynamic state. Activate HyESO2 and reset delay timer.

(3) Delay Phase: It is imperative that HyESO2 is maintained in its preset configuration t_{set} to facilitate the accommodation of overshoot dynamics upon entry into the convergence zone, thereby preventing re-exit from steady-state bounds.

(4) Steady state: Switch to HyESO1 only after completing t_{set} with $e < \zeta$.

Threshold value ζ may be empirically calibrated through operational analysis of the PMSM drive system's practical operating conditions. The maximum steady-state tracking discrepancy can be practically measured by monitoring rotational velocity across operational bandwidths. During dynamic operating regimes, transient deviation between actual and reference outputs exhibits significant magnitude superiority over steady-state counterparts, demonstrating global convergence characteristics.

Engineering practice suggests configuring ζ parameters to marginally exceed measured steady-state tracking deviations, ensuring dynamic error magnification remains below mechanical resonance excitation thresholds.

Delay time t_{set} can be obtained by either experiments or time response analysis. To better enhance the immunity of the system to the step response, according to [8], it is recommended to set the delay time t_{set} as

$$t_{set} = \frac{10}{\omega_0} \tag{31}$$

5. Experimental Results and Discussion

5.1. Introduction to Experimental Equipment

To validate the feasibility and effectiveness of the self-switching hybrid extended state observer proposed in this paper, a series of experimental tests were conducted on a permanent magnet synchronous motor drive platform. The experimental setup is shown in Figure 4, which includes two motors, two BOOSTXL DRV8305 drivers, an integrated digital signal processor TMS320F28379D, a host PC, and an oscilloscope. One motor is used to validate the algorithm proposed in this paper, while the other motor is used to provide load torque. The control algorithm was implemented in C.

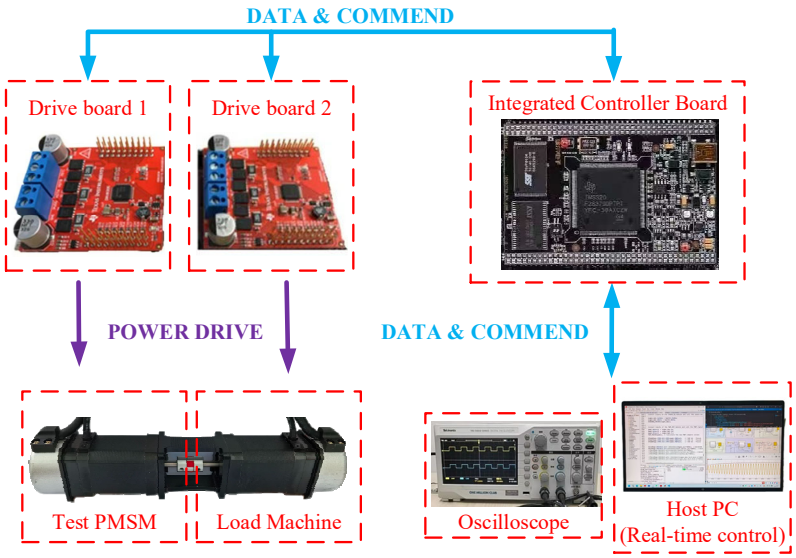


Figure 4. Testbed prototype of the PMSM.

The nominal parameters of the test motor were determined through offline identification, as shown in Table 1. The switching frequency of the inverter was set to 10 kHz. And the sampling frequency is 20 kHz. Based on the relationship between current loop bandwidth and time delay, the current loop bandwidth in PMSM drives is typically set to 1/20 of the carrier frequency. Therefore, the current loop bandwidth in the experimental system was set to 500 Hz. A digital signal processor (DSP) is used to sample the motor data, which is then transmitted to the host PC. The control algorithm runs and calculates on the host PC before being transmitted to the DSP for execution. Meanwhile, the experimental data is displayed via the host PC's upper-level computer. This implementation successfully demonstrates that the TMS320F28379D meets the minimal DSP requirements for executing the control algorithm.

Table 1. Parameters of the experimental platform.

Parameter	Value	Parameter	Value
Rated speed	1500 rpm	Flux linkage (ψ_f)	0.0164 Wb
Pole pairs (n_p)	4	Coefficient of friction (B)	3.5×10^{-4} Nm · s
Stator resistance (R_s)	0.89 Ω	Rated current	4A
Stator inductance (L_s)	0.64 mH	Rated Torque	0.2 N · m
Moment of inertia (J)	0.028 kg · cm^2	Peak Torque	0.7 N · m

To comprehensively evaluate the control performance of the proposed controller, experiments were conducted using the following methods: a current control algorithm

based on a PI controller, a traditional ADRC, and the proposed AS-HyESO. The settings of each controller are defined in Table 2.

Table 2. Parameter setting.

Experiment	Parameter	Value
PI controller	d-axis current loop proportional (p) parameter (K_{sd}^{p})	16.96
	d-axis current loop integral (I) parameter (K_{sd}^{i})	1932.08
	q-axis current loop proportional (p) parameter (K_{sq}^{p})	34.87
	q-axis current loop integral (I) parameter (K_{sq}^{i})	1932.08
Conventional ADRC	Current loop bandwidth	500 Hz
	PI controller's p parameter in d-axis (K_{p}^{d})	16.96
	PI controller's p parameter in q-axis (K_{p}^{q})	34.87
	ESO's control feedback gains matrix (G)	$\begin{bmatrix} 4 \times 10^{3} & 4 \times 10^{6} \end{bmatrix}^{T}$
	Coefficient of the control input in d-axis (α_{d0})	111.11
	Coefficient of the control input in q-axis (α_{q0})	54.05
AS-HyESO	Current loop bandwidth	500 Hz
	State feedback gain matrix (Θ_k)	$\begin{bmatrix} -5 & -0.001 \end{bmatrix}$
	Bandwidth of the AS-HyESO (ω_0)	100–6100 rad/s

5.1.1. Control Performance of Different Observer Bandwidths Across Full-Speed Range During Motor Startup and Loading

To investigate the impact of varying observer bandwidths on dynamic performance and disturbance rejection, experiments were conducted with controller coefficients set to $\Theta_k = \begin{bmatrix} -5 & -0.001 \end{bmatrix}$, and observer bandwidths were selected as 500 rad/s, 1050 rad/s, and 3200 rad/s for no-load motor startup tests.

Experimental results demonstrate that the HyESOBC proposed in this study enables stable motor operation across the full speed range, achieving zero-deviation tracking of the actual speed to the reference value. Figures 5 and 6 show the detail of the experimental curves. In the figure, the yellow curve represents the given value for the test content, while the lines in other colors represent the actual sampled values. Figure 5a reveals that, with a lower hybrid extended state observer bandwidth (500 rad/s), the motor achieves an overshoot-free startup; however, the rise time is 1.5 s, which is impractical for real-world engineering applications.

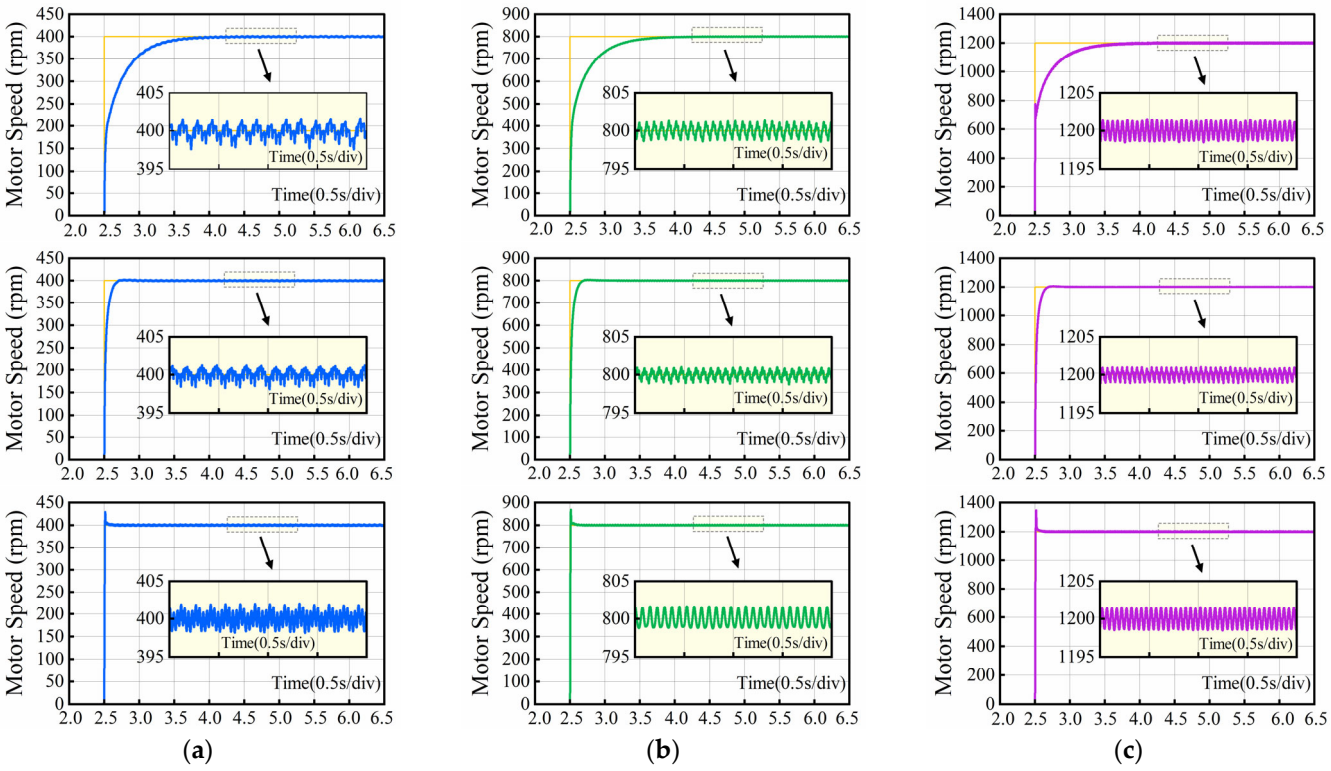


Figure 5. No-load startup experiment, from top to bottom: Step responses with reference speeds of 400 rpm, 800 rpm, and 1200 rpm. (**a**) Bandwidth of 500 rad/s. (**b**) Bandwidth of 1050 rad/s. (**c**) Bandwidth of 3200 rad/s.

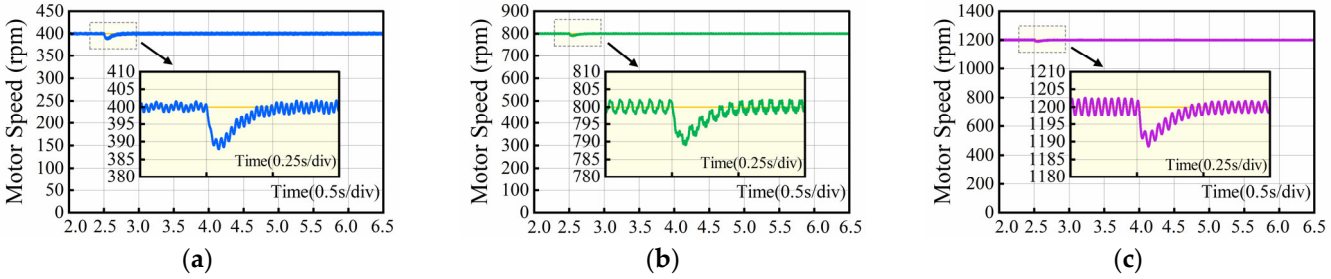


Figure 6. Sudden load application experiment at 3500 rad/s bandwidth: (**a**) Response curves at a reference speed of 400 rpm. (**b**) Response curves at a reference speed of 800 rpm. (**c**) Response curves at a reference speed of 1200 rpm.

In contrast, increasing the HyESO bandwidth to 1050 rad/s (Figure 5b) significantly reduces the no-load startup rise time to 0.15 s while maintaining overshoot-free acceleration and minimal speed ripple across the full speed range. Consequently, subsequent experiments adopt an observer bandwidth gain of 1050 rad/s for no-load startup evaluations.

Further increasing the observer bandwidth gain to 3200 rad/s (Figure 5c) shortens the rise time to 0.1 s due to the high-gain observer's rapid estimation of speed errors, which enhances the closed-loop system's dynamic gain and accelerates the regulation process. However, this higher bandwidth introduces adverse effects, including excessive overshoot and pronounced speed oscillations during startup caused by amplified noise, rendering it unsuitable for specific engineering scenarios.

Notably, Figure 6a–c illustrate that, under varying reference speeds with a 0.5 p.u. load applied at 4 s, higher observer bandwidth effectively improves the system's disturbance rejection capability. The motor speed drop remains below 10 rpm, validating the HyE-SOBC's robustness against disturbances in practical applications. Based on these findings,

an observer bandwidth gain of 3500 rad/s is selected for subsequent experiments involving sudden load application and removal.

5.1.2. Comparative Verification Under Speed Change

Figure 7 demonstrates the comparative experimental results of three different control schemes under speed variations. From Figure 7, it can be observed that, when the speed changes abruptly, the current exhibits significant overshoot, which occurs because the system adopts maximum torque during speed variations to enhance speed dynamic response performance. From Figure 7, it is evident that, compared with the PI controller and conventional ADRCler, the AS-HyESOBC achieves shorter rise time in speed regulation processes, smaller speed fluctuation ranges, and effective disturbance suppression at different speeds. Furthermore, it can also be observed that, benefiting from its single-loop control structure, the AS-HyESOBC eliminates the information loss problem caused by different sampling periods between the speed outer loop and current inner loop in traditional PI control. Its control law enables rapid estimation and real-time status updating of motor speed and q-axis current, thereby achieving transition states without overshoot during speed regulation processes. Therefore, the AS-HyESOBC exhibits excellent dynamic performance and adaptability to speed variations.

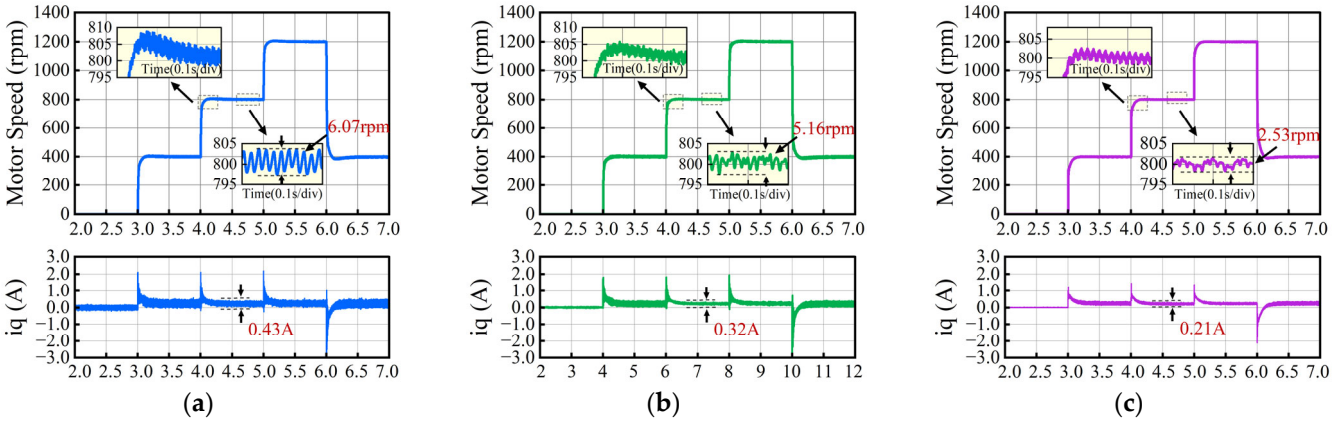


Figure 7. Comparative experimental results of no-load speed regulation under different control algorithms. From top to bottom: Motor speed, q-axis current. (**a**) Conventional PI control. (**b**) Conventional ADRC. (**c**) AS-HyESOBC.

5.1.3. Comparative Verification Under Load Torque Change

Figure 8 and Table 3 demonstrate comparative experimental results of three different control schemes under load torque step variations. Compared with the PI controller and conventional ADRCler, the self-switching HyESOBC proposed in this paper exhibits significant technical advantages. Experimental data indicate that, under sudden 0.5 pu load conditions, the speed recovery time of AS-HyESOBC (0.18 s) is reduced by 62.3% and 41.2% compared to conventional PI control (0.48 s) and conventional ADRC (0.31 s), respectively. Furthermore, the transient speed drop value of AS-HyESOBC is strictly limited within 1.2% of the rated value, significantly outperforming the 4.8% observed in PI control and 2.7% in ADRC.

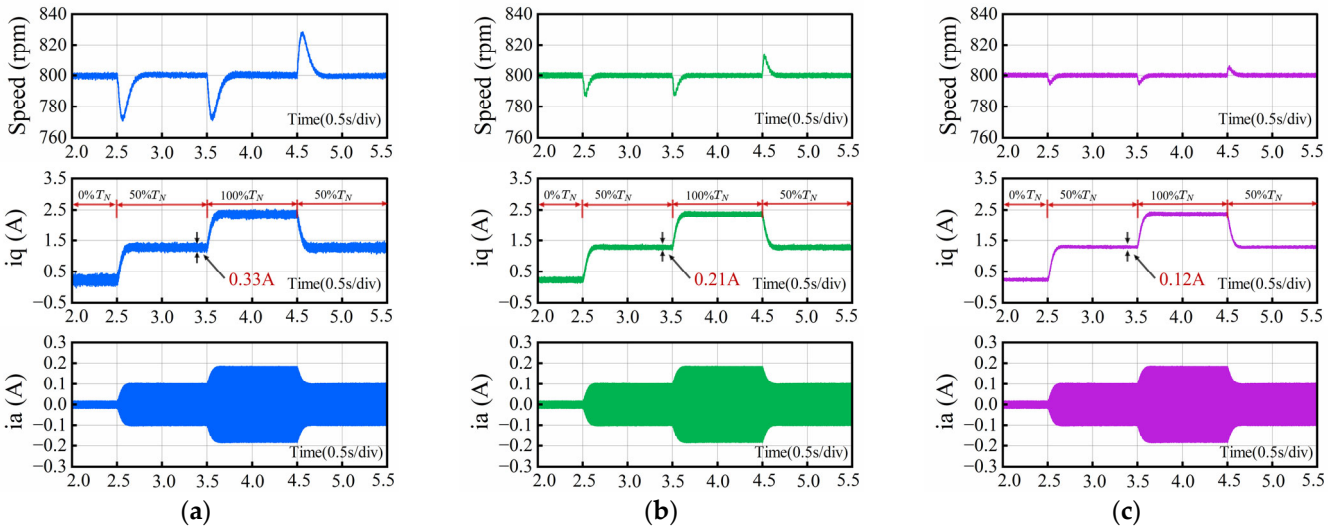


Figure 8. Comparative experimental results of three different control algorithms under load torque variations. From top to bottom: Motor speed, q-axis current. (**a**) Conventional PI control. (**b**) Conventional ADRC. (**c**) AS-HyESO.

Table 3. Detailed experimental results in Section 5.1.3.

Strategy	Speed Drop	Speed Up	Average Speed Recovery Time
Conventional PI control	28 rpm	26 rpm	0.48 s
Conventional ADRC	17 rpm	15 rpm	0.31 s
AS-HyESO	9 rpm	6 rpm	0.18 s

The improvement in dynamic characteristics originates from AS-HyESOBC's unique single-loop control structure and the designed control law. Through the Hurwitz stability criterion, the system achieves rapid response tracking to reference inputs while effectively decoupling the strong coupling effects between electromagnetic torque and mechanical dynamics during load torque transient processes.

5.1.4. Steady-State Performance Comparative Verification

Figure 9 and Table 4 present the comparative experimental results of three distinct controllers under a motor speed reference of 800 rpm and 50% rated load torque. Each control method demonstrates precise tracking performance of the q-axis current reference while maintaining undistorted sinusoidal phase currents.

Table 4. Detailed experimental results in Section 5.1.4.

Strategy	Phase-A Current THD	q-Axis Current Ripple
Conventional PI control	9.6%	0.33 A
Conventional ADRC	4.46%	0.21 A
AS-HyESO	3.37%	0.12 A

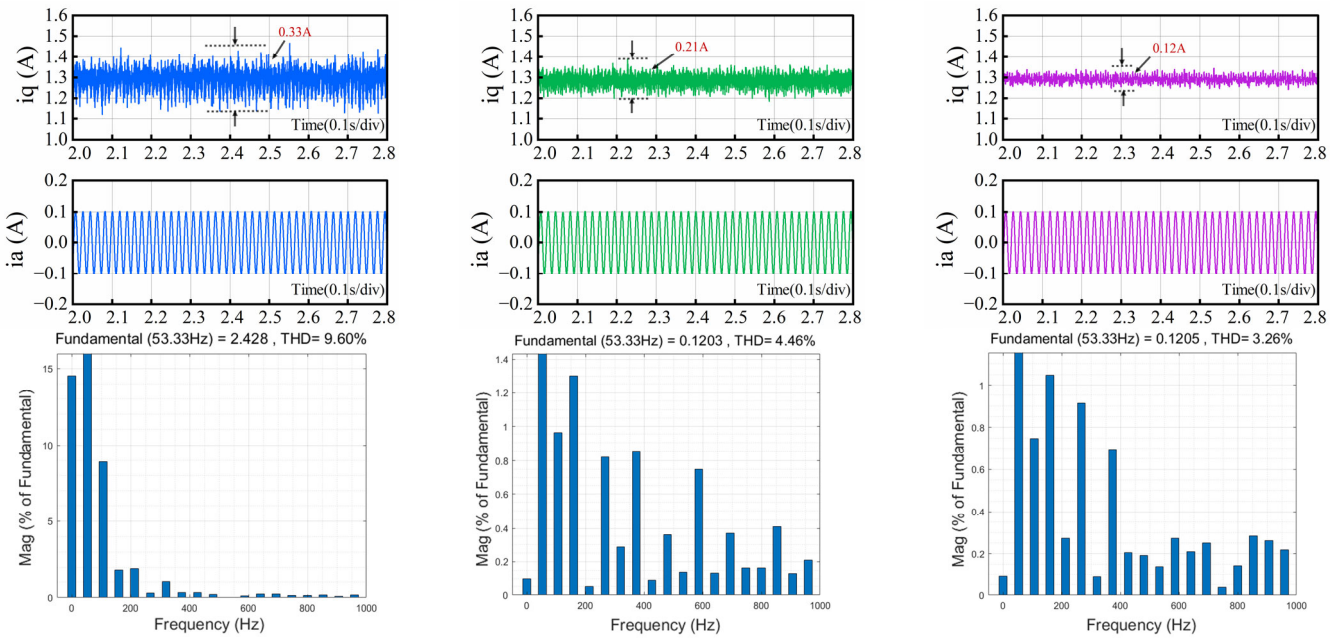


Figure 9. Comparative experimental results of three different control algorithms under 50% rated load torque. From top to bottom: q-axis current, phase-A current, phase-A current Fourier analysis. (**a**) Conventional PI control. (**b**) Conventional ADRC; (**c**) AS-HyESOBC.

As illustrated in Figure 9a, the PI controller exhibits intolerable ripple in the q-axis current. Fourier analysis of the phase-A current reveals a total harmonic distortion (THD) of 9.6%. In contrast, the conventional ADRC, shown in Figure 9b, partially suppresses current ripple, reducing the q-axis current ripple and lowering the phase-A current THD to 4.46%. However, due to the limited bandwidth of the ESO, the conventional ADRC struggles to effectively mitigate periodic disturbances.

When employing the proposed AS-HyESOBC, as depicted in Figure 9c, the current ripple is significantly suppressed, with the THD further reduced to 3.37%. These results demonstrate that AS-HyESOBC outperforms both the PI controller and conventional ADRC in terms of current ripple suppression.

5.1.5. Parameter Robustness Experiments

To address the challenges posed by variations in electrical and mechanical parameters during the quantitative simulation of PMSM operation, a feasible alternative is to adjust the motor parameters in the controller. This experiment aims to investigate the robustness of the proposed method under dynamic changes in motor system parameters. The nominal motor parameters listed in Table 1 are defined as P = {R_0, L_0}, with the reference speed set to 800 rpm. Subsequently, the motor parameters in the designed controller are set to 0.7P and 1.3P, respectively, to evaluate parameter robustness.

The experimental results shown in Figure 10 demonstrate that, after switching the observer bandwidth to HyESO1, the motor maintains stable operation even when there is a significant deviation between the controller's motor parameters and their nominal values, with no notable changes in speed ripple or q-axis current. This indicates that the proposed AS-HyESOBC exhibits exceptional robustness against motor parameter variations.



Figure 10. The response curves under parameter mismatch: (**a**) Speed curve; (**b**) iq curve.

6. Conclusions

This paper proposes an adaptive switching control strategy based on a Hybrid Extended State Observer (HyESO), termed AS-HyESO, to address the suppression of multi-channel uncertain disturbances in single-loop control systems for Permanent Magnet Synchronous Motors (PMSMs). By decoupling the estimation of matched disturbances (control channel) and unmatched disturbances (non-control channels) and designing a composite feedback control law for coordinated compensation, the HyESO achieves precise observation and dynamic elimination of complex disturbances. To resolve the inherent trade-off between dynamic response and disturbance rejection robustness in conventional high-gain ESO designs, the proposed adaptive bandwidth switching mechanism employs a lower bandwidth during transient processes to suppress overshoot and switches to a higher bandwidth in steady-state operation to enhance disturbance rejection capability. This approach unifies overshoot-free speed tracking with robust anti-disturbance performance. Experimental validation on a 64 W PMSM dual-motor platform demonstrates significant improvements in control performance under complex operating conditions, including speed transients and load variations. Both theoretical analysis and experimental results confirm that AS-HyESO, through its structural innovation and adaptive parameter optimization, provides a universal solution for single-loop PMSM control systems that balances dynamic performance and steady-state precision. This work holds substantial reference value for high-precision motor drive applications.

Author Contributions: Conceptualization, W.L.; Software, J.W.; Investigation, Y.Q.; Writing—original draft, W.L., Y.Q. and J.W.; Supervision, W.Z.; Funding acquisition, W.Z. All authors have read and agreed to the published version of the manuscript.

Funding: This research was funded by National Natural Science Foundation of China grant number 52207043.

Data Availability Statement: The original contributions presented in the study are included in the article, further inquiries can be directed to the corresponding author.

Conflicts of Interest: The authors declare no conflict of interest.

Nomenclature

Abbreviations

ESO	Extended state observer
ESOBC	Extended state observer-based control
ADRC	Active disturbance rejection control
AS-HyESO	Hybrid extended state observer with adaptive switching strategy
AS-HESOBC	Hybrid extended state observer-based control with adaptive switching strategy
HyESO	Hybrid extended state observer
GESO	Generalized extended state observer
PMSM	Permanent magnet synchronous motor

Symbols

ω_m	Angular velocity	r/min	n_p	Pole pairs	\

i_{dq}	dq-axe current	A	R_s	Stator resistance	Ω
u_{dq}	dq-axe voltage	V	ψ_f	Permanent magnet flux	Wb
$d_{(\cdot)-total}$	Total disturbance	\	B	Viscous friction coefficient	Nm·s
$d_{(\cdot)-ap}$	Aperiodic disturbances	\	L_s	Synchronous inductance	mH
$d_{(\cdot)-p}$	Periodic disturbances	\	J	Total inertia	kg·cm^2
$\Delta_{(\cdot)-ap}$	Unknown aperiodic disturbances	\	T_L	load torque	N·m
u	Control input	r/min	K_t	Torque constant	Wb
α	Coefficient of the control input	\	y	Control output	r/min
$f(\cdot)$	System's lumped disturbance	\	x	State variables	\
β	ESO's feedback control gains	\	z, $\hat{x}$	Estimated state variables	\
k	Gain vector of the nominal state feedback controller	\	e	Composite error of the integrated system	\
L_m	Matched observer gain	\	L_{mm}	Mismatched observer gain	\
Θ_r	Reference input gain	\	Θ_d	Disturbance compensation gain	\
Θ_k	State feedback gain	\	ω_0	Bandwidth of the AS-HyESO	rad/s
L	AS-HyESO's observer gain	\	ζ	Threshold value	r/min
flag	Speed change flag	\	t_{set}	Preset configuration	s

References

1. Peng, Y.; Chen, F.; Chen, F.; Wu, C.; Wang, Q.; He, Z.; Lu, S. Energy-Efficient Train Control: A Comparative Study Based on Permanent Magnet Synchronous Motor and Induction Motor. *IEEE Trans. Veh. Technol.* **2024**, *73*, 16148–16159. [CrossRef]
2. Zhang, Z.; Ma, R.; Wang, L.; Zhang, J. Novel PMSM Control for Anti-Lock Braking Considering Transmission Properties of the Electric Vehicle. *IEEE Trans. Veh. Technol.* **2018**, *67*, 10378–10386. [CrossRef]
3. Rodríguez-Nieto, D.; Navas, E.; Fernández, R. Automated Seeding in Hydroponic Greenhouse With a Dual-Arm Robotic System. *IEEE Access* **2025**, *13*, 30745–30761. [CrossRef]
4. Hong, D.K.; Hwang, W.; Lee, J.Y.; Woo, B.C. Design, Analysis, and Experimental Validation of a Permanent Magnet Synchronous Motor for Articulated Robot Applications. *IEEE Trans. Magn.* **2018**, *54*, 8201304. [CrossRef]
5. Yang, J.; Chen, W.H.; Li, S.; Guo, L.; Yan, Y. Disturbance/Uncertainty Estimation and Attenuation Techniques in PMSM Drives—A Survey. *IEEE Trans. Ind. Electron.* **2017**, *64*, 3273–3285. [CrossRef]
6. Tian, M.; Wang, B.; Yu, Y.; Dong, Q.; Xu, D. Adaptive Active Disturbance Rejection Control for Uncertain Current Ripples Suppression of PMSM Drives. *IEEE Trans. Ind. Electron.* **2024**, *71*, 2320–2331. [CrossRef]
7. Li, X.; Tian, W.; Gao, X.; Yang, Q.; Kennel, R. A Generalized Observer-Based Robust Predictive Current Control Strategy for PMSM Drive System. *IEEE Trans. Ind. Electron.* **2022**, *69*, 1322–1332. [CrossRef]

8. Zhu, S.; Huang, W.; Zhao, Y.; Lin, X.; Dong, D.; Jiang, W.; Zhao, Y.; Wu, X. Robust Speed Control of Electrical Drives With Reduced Ripple Using Adaptive Switching High-Order Extended State Observer. *IEEE Trans. Power Electron.* **2022**, *37*, 2009–2020. [CrossRef]
9. Qu, L.; Qiao, W.; Qu, L. Active-Disturbance-Rejection-Based Sliding-Mode Current Control for Permanent-Magnet Synchronous Motors. *IEEE Trans. Power Electron.* **2021**, *36*, 751–760. [CrossRef]
10. Liu, Y.C.; Laghrouche, S.; Depernet, D.; N'Diaye, A.; Djerdir, A.; Cirrincione, M. Disturbance-observer-based speed control for SPMSM drives using modified super-twisting algorithm and extended state observer. *Asian J. Control* **2024**, *26*, 1089–1102. [CrossRef]
11. Yao, Y.; Zhuang, Y.; Xie, Y.; Xu, P.; Wu, C. Prescribed Performance Global Non-Singular Fast Terminal Sliding Mode Control of PMSM Based on Linear Extended State Observer. *Actuators* **2025**, *14*, 65. [CrossRef]
12. Liu, J.; Yang, J.; Li, S.; Wang, X. Single-Loop Robust Model Predictive Speed Regulation of PMSM Based on Exogenous Signal Preview. *IEEE Trans. Ind. Electron.* **2023**, *70*, 12719–12729. [CrossRef]
13. Tu, W.; Luo, G.; Chen, Z.; Liu, C.; Cui, L. FPGA Implementation of Predictive Cascaded Speed and Current Control of PMSM Drives With Two-Time-Scale Optimization. *IEEE Trans. Ind. Inform.* **2019**, *15*, 5276–5288. [CrossRef]
14. Bolognani, S.; Bolognani, S.; Peretti, L.; Zigliotto, M. Design and Implementation of Model Predictive Control for Electrical Motor Drives. *IEEE Trans. Ind. Electron.* **2009**, *56*, 1925–1936. [CrossRef]
15. Li, S.; Yang, J.; Chen, W.H.; Chen, X. Generalized Extended State Observer Based Control for Systems With Mismatched Uncertainties. *IEEE Trans. Ind. Electron.* **2012**, *59*, 4792–4802. [CrossRef]
16. Kazmierkowski, M.P. Electric motor drives: Modeling, analysis and control, R. Krishan, Prentice-Hall, Upper Saddle River, NJ, 2001, xxviii + 626 pp. ISBN 0-13-0910147. *Int. J. Robust Nonlinear Control* **2004**, *14*, 767–769. [CrossRef]
17. Yang, F.; Jiang, F.; Xu, Z.; Qiu, L.; Xu, B.; Zhang, Y.; Yang, K. Complex Coefficient Active Disturbance Rejection Controller for Current Harmonics Suppression of IPMSM Drives. *IEEE Trans. Power Electron.* **2022**, *37*, 10443–10454. [CrossRef]
18. Liu, C.; Luo, G.; Duan, X.; Chen, Z.; Zhang, Z.; Qiu, C. Adaptive LADRC-Based Disturbance Rejection Method for Electromechanical Servo System. *IEEE Trans. Ind. Appl.* **2020**, *56*, 876–889. [CrossRef]
19. Gao, Z. Scaling and bandwidth-parameterization based controller tuning. In Proceedings of the 2003 American Control Conference, Denver, CO, USA, 4–6 June 2003; Volume 6, pp. 4989–4996. [CrossRef]
20. Zhang, Y.; Jin, J.; Huang, L. Model-Free Predictive Current Control of PMSM Drives Based on Extended State Observer Using Ultralocal Model. *IEEE Trans. Ind. Electron.* **2021**, *68*, 993–1003. [CrossRef]
21. Han, J. From PID to Active Disturbance Rejection Control. *IEEE Trans. Ind. Electron.* **2009**, *56*, 900–906. [CrossRef]
22. Lv, S.; Peng, K.; Wang, H.; Zhang, H. H_∞ Filter and Extended State Observer-Based Disturbance Rejection Control for Systems With Uncertainty and Noise. *IEEE Trans. Circuits Syst. I Regul. Pap.* **2025**, 1–9. [CrossRef]

Disclaimer/Publisher's Note: The statements, opinions and data contained in all publications are solely those of the individual author(s) and contributor(s) and not of MDPI and/or the editor(s). MDPI and/or the editor(s) disclaim responsibility for any injury to people or property resulting from any ideas, methods, instructions or products referred to in the content.